Report

Current Biology

Unmasking Transcriptional Heterogeneity in Senescent Cells

Highlights

- The transcriptome of senescent cells is highly heterogeneous
- Senescence transcriptome programs depend on the cell type and stress
- Gene expression in senescent cells is temporally dynamic
- We identified 55 genes at the core of the senescence-associated transcriptome

Authors

Alejandra Hernandez-Segura, Tristan V. de Jong, Simon Melov, Victor Guryev, Judith Campisi, Marco Demaria

Correspondence

m.demaria@umcg.nl

In Brief

The phenotype of senescent cells is highly heterogeneous, but reasons for this variability are poorly understood. Hernandez-Segura et al. identify senescence transcriptome signatures that are strongly associated with specific stresses and cell types and show that the gene expression profiles of various senescence programs are highly dynamic.

Hernandez-Segura et al., 2017, Current Biology *27*, 1–9
September 11, 2017
http://dx.doi.org/10.1016/j.cub.2017.07.033

CellPress

Please cite this article in press as: Hernandez-Segura et al., Unmasking Transcriptional Heterogeneity in Senescent Cells, Current Biology (2017), http://dx.doi.org/10.1016/j.cub.2017.07.033

Current Biology
Report

Unmasking Transcriptional Heterogeneity in Senescent Cells

Alejandra Hernandez-Segura,[1] Tristan V. de Jong,[1] Simon Melov,[2] Victor Guryev,[1] Judith Campisi,[2,3] and Marco Demaria[1,4,*]

[1]European Research Institute for the Biology of Aging, University of Groningen, University Medical Center Groningen, Antonius Deusinglaan 1, 9713 AV Groningen, the Netherlands

[2]Buck Institute for Research on Aging, 8001 Redwood Boulevard, 94945 Novato CA, USA

[3]Lawrence Berkeley National Laboratory, Life Sciences Division, 1 Cyclotron Road, Berkeley, CA 94720, USA

[4]Lead Contact

*Correspondence: m.demaria@umcg.nl

http://dx.doi.org/10.1016/j.cub.2017.07.033

SUMMARY

Cellular senescence is a state of irreversibly arrested proliferation, often induced by genotoxic stress [1]. Senescent cells participate in a variety of physiological and pathological conditions, including tumor suppression [2], embryonic development [3, 4], tissue repair [5–8], and organismal aging [9]. The senescence program is variably characterized by several non-exclusive markers, including constitutive DNA damage response (DDR) signaling, senescence-associated β-galactosidase (SA-βgal) activity, increased expression of the cyclin-dependent kinase (CDK) inhibitors p16INK4A (*CDKN2A*) and p21CIP1 (*CDKN1A*), increased secretion of many bio-active factors (the senescence-associated secretory phenotype, or SASP), and reduced expression of the nuclear lamina protein LaminB1 (*LMNB1*) [1]. Many senescence-associated markers result from altered transcription, but the senescent phenotype is variable, and methods for clearly identifying senescent cells are lacking [10]. Here, we characterize the heterogeneity of the senescence program using numerous whole-transcriptome datasets generated by us or publicly available. We identify transcriptome signatures associated with specific senescence-inducing stresses or senescent cell types and identify and validate genes that are commonly differentially regulated. We also show that the senescent phenotype is dynamic, changing at varying intervals after senescence induction. Identifying novel transcriptome signatures to detect any type of senescent cell or to discriminate among diverse senescence programs is an attractive strategy for determining the diverse biological roles of senescent cells and developing specific drug targets.

RESULTS AND DISCUSSION

Specific senescence-associated transcriptome programs have been mainly characterized in fibroblasts. We, therefore, constructed a signature based on whole-transcriptome profiles of various strains of human fibroblasts subjected to different senescence-inducing stimuli. To increase statistical power, and limit biases associated with individual studies [11], we used several datasets generated at different times and in different laboratories, including ours. Only datasets generated using primary fibroblasts without genetic manipulation (with the exception of oncogenic Ras expression in the case of oncogene-induced senescence), with at least two biological replicates, and at least 50% of the cells positive for senescence-associated β-galactosidase (SA-βgal) activity, were included in the analysis (Data S1A). The selected datasets covered 6 different fibroblast strains (BJ, IMR90, HFF, MRC5, WI38, and HCA-2) and 3 different senescence-inducing stimuli (replicative senescence [RS], oncogene-induced senescence [OIS], and ionizing radiation-induced senescence [IRIS]) and were generated by 5 independent laboratories (Figure 1A) [12–16].

Principal-component analysis (PCA) revealed that the tissue of origin (lung or foreskin) accounted for most of the variation (data not shown). However, the second and third principal components separated the cells according to senescence status, with some influence from the study/dataset of origin (Figure S1A). Nonetheless, one sample within one of the datasets (RS IMR90 [14]) clustered differently from its replicates. The aberrant clustering of this sample was reported in the original study, and this sample was then removed from further analysis (Figure S1A).

Each sample showed transcriptional induction of at least some of the known senescence-associated genes, namely, p16INK4A (*CDKN2A*), p21CIP1 (*CDKN1A*), *GLB1* (SA-βgal), and several senescence-associated secretory phenotype (SASP) factors (Figure S1B). Interestingly, our analysis revealed variability due to intra- and inter-laboratory culture conditions (Figure S1B).

We first grouped the datasets based on the senescence stimulus (Figure 1A). For RS, the only group with more than one dataset, we performed a meta-analysis combining three different methods: we used (1) a negative binomial-generalized linear model (NB-GLM), pooling all the samples in all the datasets for one particular senescence-inducing stimulus and comparing them to proliferating counterparts, and within the model, we included a covariate that accounted for inter-laboratory and inter-strain differences (see STAR Methods for details); (2) an analysis of each individual dataset and subsequent combination of the p values using the Fisher method; and (3) an inverse-normal

A

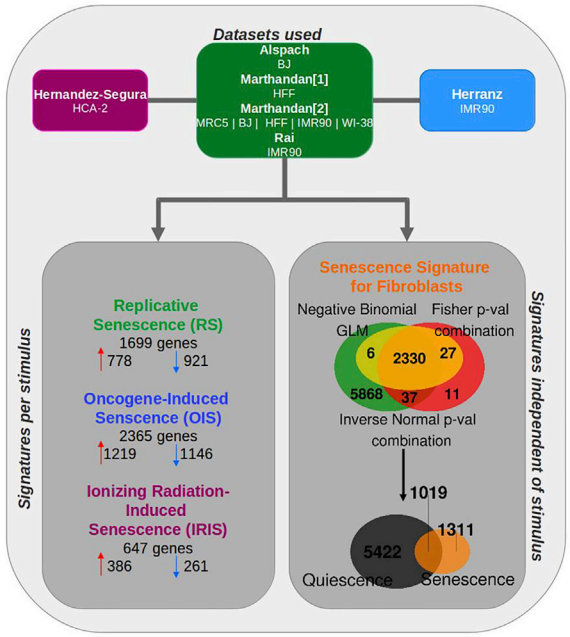

C

P-value	Pathway	Source
	Downregulated	
7.2E-10	Gene Expression	Reactome
6.4E-09	Chromatin modifying enzymes	Reactome
6.4E-09	Chromatin organization	Reactome
2.9E-06	Generic Transcription Pathway	Reactome
4.1E-06	HATs acetylate histones	Reactome
5.4E-06	AndrogenReceptor	NetPath
1.7E-05	Regulation of Androgen receptor activity	PID
1.9E-05	Histone Modifications	Wikipathways
5.3E-05	Androgen receptor signaling pathway	Wikipathways
1.4E-04	DNA Repair	Reactome
	Upregulated	
8.4E-11	Membrane Trafficking	Reactome
3.3E-10	Vesicle-mediated transport	Reactome
8.8E-09	Intra-Golgi and retrograde Golgi-to-ER traffic	Reactome
5.3E-08	Asparagine N-linked glycosylation	Reactome
8.4E-07	ER to Golgi Anterograde Transport	Reactome
5.7E-06	Transport to the Golgi and subsequent modification	Reactome
1.7E-05	Retrograde transport at the Trans-Golgi-Network	Reactome
2.6E-05	Golgi-to-ER retrograde transport	Reactome
2.6E-05	Protein processing in endoplasmic reticulum - Homo sapiens (human)	KEGG
4.5E-05	Activation of NF-kappaB in B cells	Reactome

B

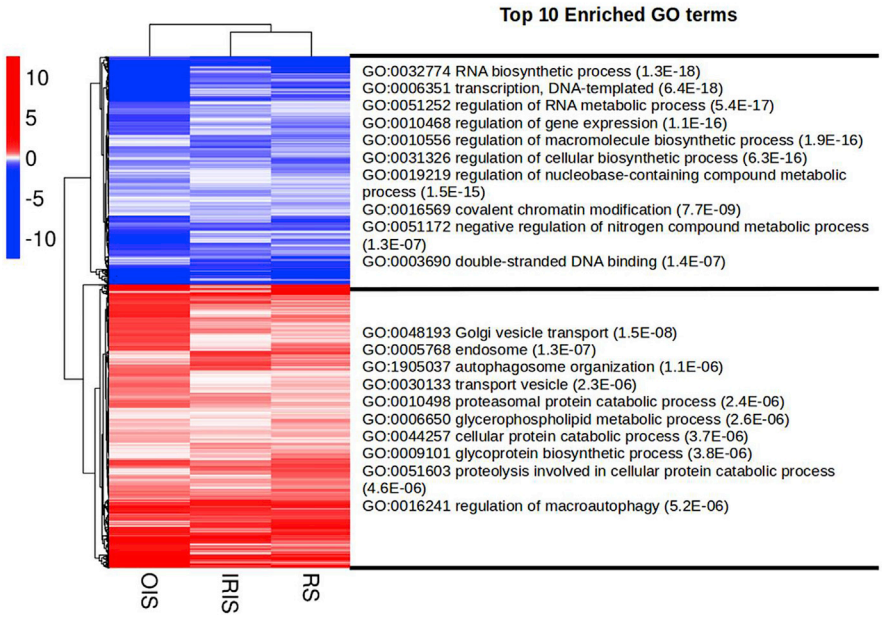

Figure 1. Meta-Analysis of Senescent Fibroblast Transcriptomics

(A) Experimental design. Seven RNA-seq datasets obtained from the indicated studies were used to build a stimulus-specific signature and general signature of senescent fibroblasts, regardless of the stimulus. Only genes with a $p \leq 0.01$, calculated by the three methods and with expression unchanged or in the opposite direction in quiescence, were included in each signature. The number of genes constituting each signature is displayed in the flower plot.

(B) Heatmap of the 1,311 genes in the senescence signature of fibroblasts and the top 10 enriched GO terms. The graph shows the logarithm base 2 of the fold change for each senescence-inducing stimulus tested with respect to proliferating cells. Blue indicates downregulated genes; red indicates upregulated genes.

(C) Top 10 enriched pathways in the senescence signature of fibroblasts. The pathways enriched in genes within the senescence signature of fibroblasts (in B) are enlisted with their corresponding p value and source. ER, endoplasmic reticulum. HAT, histone acetyltransferases; KEGG, Kyoto Encylopedia of Genes and Genomes; PID, Pathway Interaction Database.

See also Figure S1 and Data S1.

p value combination technique in which each dataset was weighted according to the number of replicates [17, 18]. We set a stringent threshold of nominal $p \leq 0.01$ to reduce the odds of false-positive results and retained only those genes that were differentially expressed by the three different methods. For IRIS and OIS, where only one dataset for each condition was

available, we used a normal differential expression analysis to select genes (adjusted $p \leq 0.01$). To ensure the identification of genes associated with senescence, and not growth arrest per se, we analyzed quiescent (HCA2) fibroblasts and removed from subsequent analysis those genes similarly regulated in both quiescence and each of the senescence conditions.

A number of genes were associated with a specific senescence-inducing stimulus: 1,699 genes with RS, 2,365 genes with OIS, and 647 genes with IRIS (Figures 1A and S1C; Data S1B–S1D). Of note, the stimulus-specific signature might be influenced by the fact that more than one dataset was available only for RS. However, common differentially expressed genes between the different stimuli were not affected by this variable. Thus, we performed a meta-analysis using the same three methods described for the stimulus-specific signatures but pooled all the datasets available and compared senescent cells (regardless of the stimulus) to proliferating cells. We found that 2,330 genes were differentially expressed by senescent fibroblasts, regardless of the senescence inducer, and half of these genes (1311 genes) were not shared with quiescent cells (Figure 1A; Data S1E). Within the senescence-associated signature of fibroblasts, multiple genes related to transcription and RNA synthesis were downregulated, while genes involved in vesicle transport were upregulated (Figure 1B). Among the main gene ontology (GO) pathways [19, 20] showing altered in senescent cells, "chromatin organization," "DNA repair," "membrane trafficking," and "activation of NF-kappaB" were notable for their known links to senescence and aging (Figure 1C) (Figure 1C) [1, 10, 21, 22].

An important contributor to the heterogeneity of the senescence program is the expression of cell-type-specific genes [23]. For example, upregulation of various components of the SASP has been reported to be dependent on the type of cell [24]. To identify variability due to cell type and identify genes at the core of the senescence program, we used datasets from melanocytes, keratinocytes, and astrocytes. We used inclusion criteria similar to those used for the fibroblast datasets (Data S2A). The datasets from melanocytes and keratinocytes were obtained in our laboratory: the cells were induced to senescence by IRIS, RNA was collected 10 days after induction, and senescence status was confirmed by SA-βgal activity and growth arrest (Figure S2A). The dataset from astrocytes was publicly available, and senescence was induced by oxidative stress [25] (Figure 2A).

To identify cell-type-dependent and -independent senescence signatures, we compared the lists of differentially expressed genes in the three cell types with the senescence-specific signature derived from fibroblasts (Figure 2A; Data S2B–S2E). Cell-type-dependent genes were enriched in different GO terms. For instance, few GO terms related to intracellular transport, RNA and/or protein expression, or processing and immune system functions were associated with the different cell types (Figure S2B). Three of the enriched GO terms for either astrocytes or keratinocytes were associated with differentiation in their tissue of origin (namely, "neurogenesis" or "neuron differentiation" and "epithelial cell differentiation," respectively).

Importantly, upon examining the list of common differentially expressed genes, we identified a significant number of hits (55 in total; Figure 2B; Data S2F) comprising a senescence core signature. Remarkably, none of the classical senescence markers (*CDKN2A*, *CDKN1A*, *LMNB1*, and members of the SASP) were among these hits, since either they were not differentially expressed in all the cell types, or they were shared with quiescence (Figure S2C). Nevertheless, within the senescence core signature, we found genes that had been previously linked to senescence: *BCL2L2* (also known as Bcl-w), a negative regulator of apoptosis [26]; *PATZ1*, a transcriptional repressor whose expression inhibits senescence in endothelial cells [27]; *SMO*, a component of the Hedgehog pathway [28]; and *CCND1*, a regulatory subunit of CDK4 or CDK6, whose activity is required for the G1/S transition [29]. Moreover, a number of other genes in the signature were reported to be implicated in oncogenesis or in known senescence-associated pathways (see Data S2G). In terms of GO and pathway analysis, some of the downregulated genes were associated with DNA binding or regulation of transcription, while upregulated genes were mainly related to DNA damage checkpoints and mitosis (Figures 2C and 2D). Of note, most of the genes had a moderate fold change, yet 26 of them changed greater than 1.3-fold in all cell types.

From this senescence-associated core signature, we selected a number of genes for further validation using qPCR and human BJ primary fibroblasts. We induced senescence by various means, including those used in the previous analyses (ionizing radiation, replication, and oxidative stress), as well as doxorubicin, a DNA-damaging chemotherapeutic agent known to cause senescence [30]) (Figures S3A–S3D). Senescence status was confirmed by SA-βgal activity (Figure S3A), lack of 5-ethynyl-2'-deoxyuridine (EdU) incorporation (Figure S3B), and increased expression of p16INK4a and p21CIP1 (for RS cells; Figure S3C). Furthermore, to investigate potential conservation among species, we measured the expression of a subset of genes in senescent mouse cells (mouse embryonic fibroblasts [MEFs] or neonatal endothelial cells) (Figures S3E and S3F). We confirmed the differential expression of these genes under most of the conditions tested, further validating our identification of a senescence core signature. In a few cases, the differential expression of individual genes was not statistically significant, suggesting that a combination of the expression level of senescence core genes might be a much stronger predictor of senescence. Moreover, we identified discrepancies between mouse and human cells for *EFNB3*, suggesting potential differences in senescence core signatures among species.

To validate the specificity of our senescence core signature and test its validity in predicting senescence in diseased tissues, we analyzed additional datasets. To exclude the possibility that genes in our core signature were predictors of a general response to genotoxic stress, we interrogated published datasets that used mild forms of DNA damage ([31]; GEO: GSE80207). Only one gene in our signature (*PLK3*) was reported differentially expressed in a radiosensitive lymphoblast line 4 hr after exposure to 2 Gy ionizing radiation (false discovery rate [FDR] ≤ 0.05), a dose that causes damage without pervasive permanent cell-cycle arrest. Importantly, this gene was no longer differentially expressed 24 hr or 14 days after the radiation or at any time after radiation in a radioresistant lymphoblast line (data not shown).

To understand whether genes present in the core signature were differentially regulated in diseased and senescence-enriched tissues, we used an RNA sequencing (RNA-seq) dataset

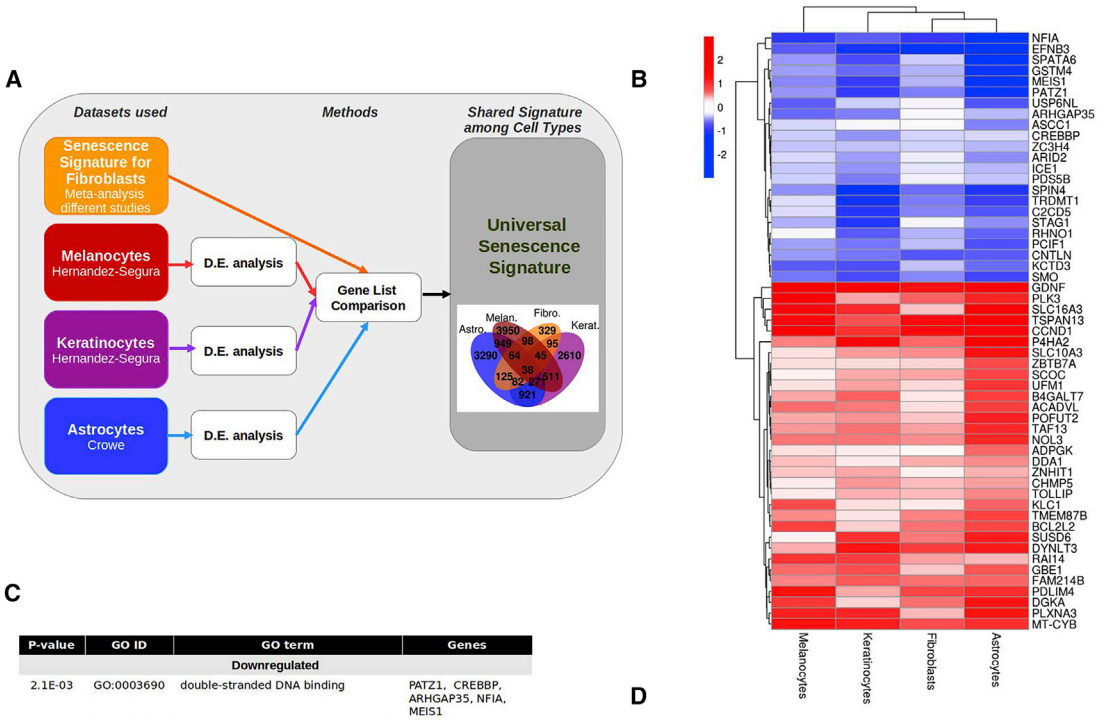

C

P-value	GO ID	GO term	Genes
		Downregulated	
2.1E-03	GO:0003690	double-stranded DNA binding	PATZ1, CREBBP, ARHGAP35, NFIA, MEIS1
2.6E-03	GO:0001077	transcriptional activator activity, RNA polymerase II core promoter proximal region sequence-specific binding	PATZ1, NFIA, MEIS1
2.7E-03	GO:0008589	regulation of smoothened signaling pathway	CREBBP, SMO
2.8E-03	GO:0000975	regulatory region DNA binding	PATZ1, CREBBP, ARHGAP35, NFIA, MEIS1
3.4E-03	GO:0051173	positive regulation of nitrogen compound metabolic process	CREBBP, SMO, NFIA, MEIS1, PATZ1, STAG1, ICE1
3.5E-03	GO:0009891	positive regulation of biosynthetic process	CREBBP, SMO, NFIA, MEIS1, PATZ1, STAG1, ICE1
6.0E-03	GO:0006304	DNA modification	TRDMT1, ASCC1
7.6E-03	GO:0043565	sequence-specific DNA binding	PATZ1, CREBBP, ARHGAP35, NFIA, MEIS1
8.1E-03	GO:0051252	regulation of RNA metabolic process	CREBBP, ARHGAP35, ARID2, ASCC1, SMO, NFIA, MEIS1, PATZ1, STAG1, ICE1
8.2E-03	GO:0006351	transcription, DNA-templated	CREBBP, ARHGAP35; ARID2, ASCC1, SMO, NFIA, MEIS1, PATZ1, STAG1, ICE1
8.50E-03	GO:0071482	cellular response to light stimulus	CREBBP, RHNO1
		Upregulated	
6.9E-03	GO:0044783	G1 DNA damage checkpoint	PLK3, CCND1
8.1E-03	GO:0007346	regulation of mitotic cell cycle	PLK3, CCND1, DYNLT3, CHMP5

D

P-value	Pathway	Source	Genes
	Downregulated		
7.8E-05	Cohesin Loading onto Chromatin	Reactome	PDS5B; STAG1
9.5E-05	Establishment of Sister Chromatid Cohesion	Reactome	PDS5B; STAG1
1.6E-04	Mitotic Telophase/Cytokinesis	Reactome	PDS5B; STAG1
1.7E-03	FOXA1 transcription factor network	PID	CREBBP, NFIA
2.0E-03	Hedgehog signaling events mediated by Gli proteins	PID	CREBBP; SMO
4.2E-03	Hedgehog	INOH	CREBBP; SMO
5.3E-03	S Phase	Reactome	PDS5B; STAG1
6.3E-03	Androgen receptor signaling pathway	Wikipathways	PATZ1; CREBBP
8.2E-03	Resolution of Sister Chromatid Cohesion	Reactome	PDS5B; STAG1
9.7E-03	Mitotic Prometaphase	Reactome	PDS5B; STAG1
	Upregulated		
1.7E-03	Photodynamic therapy-induced NF-kB survival signaling	Wikipathways	BCL2L2, CCND1
2.3E-03	inactivation of gsk3 by akt causes accumulation of b-catenin in alveolar macrophages	BioCarta	CCND1, TOLLIP
2.4E-03	miR-targeted genes in epithelium - TarBase	Wikipathways	ADPGK, RAI14, CCND1, P4HA2
7.8E-03	Glucose metabolism	Reactome	ADPGK, GBE1
9.4E-03	miR-targeted genes in lymphocytes - TarBase	Wikipathways	ADPGK, RAI14, CCND1, P4HA2

Figure 2. Characteristics of the Core Senescence-Associated Signature

(A) Experimental design. RNA-seq datasets obtained from the indicated studies of melanocytes, keratinocytes, and astrocytes were compared to the senescence signature of fibroblasts. The intersection of genes differentially expressed ($p \leq 0.01$) in all the datasets are shown in the flower plot. D.E., differential expression.

(B) Heatmap of the 55 genes of the senescence core signature. The figure shows the logarithm base 2 of the fold change for each cell type with respect to proliferating cells.

(C) GO terms enriched in the core senescence signature. The GO terms enriched in genes within the core senescence signature (in B) are listed with the corresponding p value and the associated genes.

(D) Pathways enriched in the core signature of senescence. The pathways enriched in genes within the core senescence signature (in B) are listed with their corresponding p value, source, and the associated genes. INOH, integrating network objects with hierarchies; NF-κB, nuclear factor κB; PID, Pathway Interaction Database.

See also Figures S2 and S3 and Data S2.

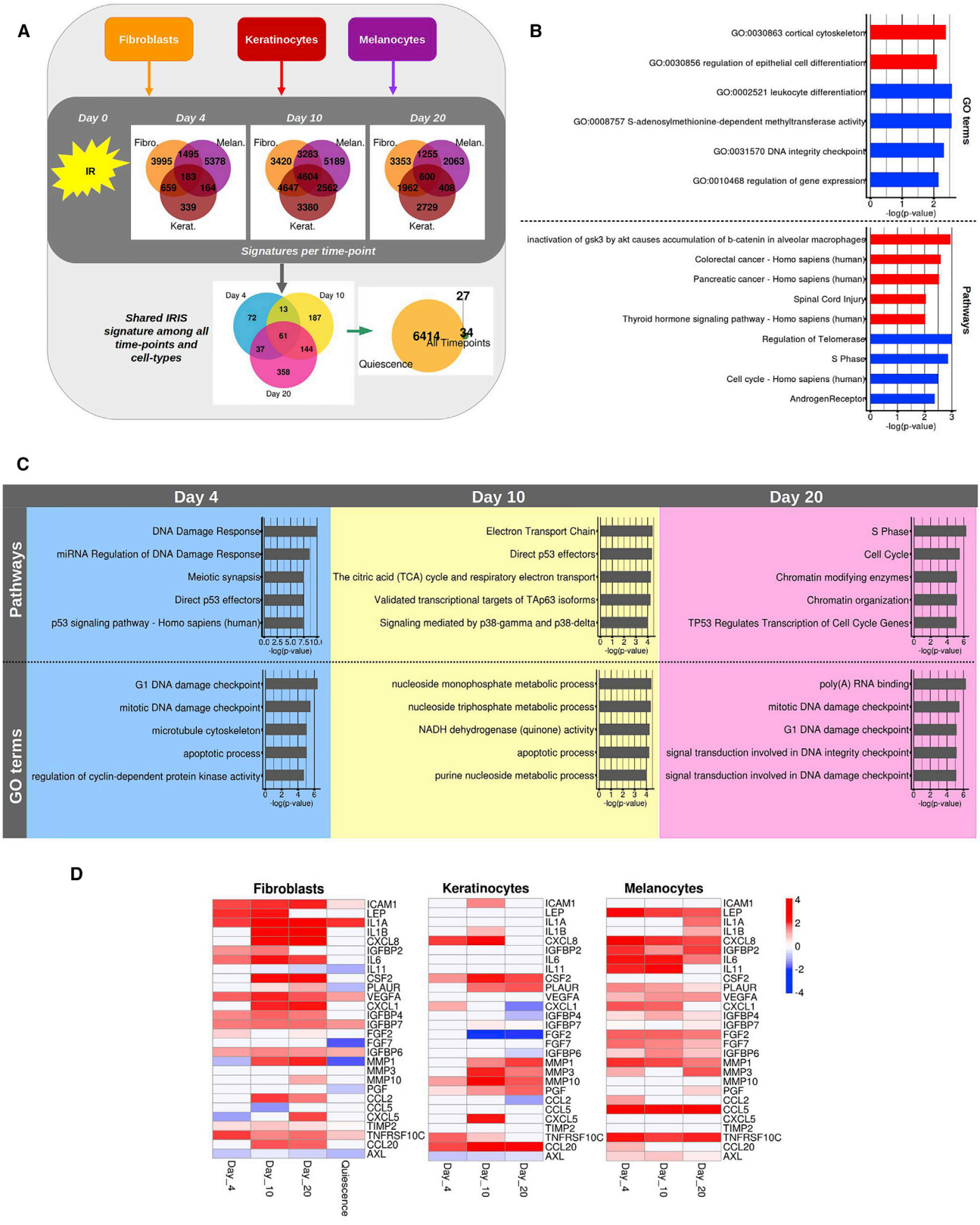

Figure 3. Temporal Dynamics of the Senescence Transcriptome

(A) Experimental design. Fibroblasts (HCA-2; yellow), melanocytes (red), and keratinocytes (magenta) were exposed to ionizing radiation (IR), and RNA was harvested 4, 10, or 20 days later. Transcriptomes of the different cell types and intervals after senescence induction were obtained by RNA-seq. A time-point

(legend continued on next page)

from lung tissues of patients with idiopathic pulmonary fibrosis, in which known senescence markers were detected [32]. Strikingly, ten genes in our core signature (*DGKA*, *GBE1*, *GDNF*, *KCTD3*, *MEIS1*, *PDLIM4*, *RAI4*, *SPIN4*, *TAF13*, and *TRDMT1*) were also present in this dataset (adjusted $p \leq 0.01$; data not shown). These findings suggest that even in whole tissues where the number of senescent cells is small (most aged or diseased tissues contained 1%–3% senescent cells [33]), some of the genes of our core signature can be identified as differentially regulated.

The senescence phenotype, including the transcriptome, is highly dynamic, and not all the common senescence markers appear or persist simultaneously [34, 35]. However, most studies analyze senescent phenotypes 7–10 days after applying the senescence inducers [36, 37]. To explore the temporal dynamics of senescence-associated gene expression, we generated RNA-seq datasets using fibroblasts (HCA-2), melanocytes, and keratinocytes (6 biological replicates each) at 4 (early), 10 (intermediate) and 20 (late) times after ionizing radiation (Figure 3A; Data S3A–S3C). We identified 61 genes that were shared among all cell types and time points, 34 of which were not shared with quiescent cells (Figure S4A; Data S3D). GO annotations and pathway analysis revealed the differential regulation of genes involved in cancer and cell-cycle progression (Figure 3B).

We then obtained transcriptomic signatures that were specific for each time point to determine the dynamics of the response to a senescence-inducing stimulus (Figure 3C; Data S3A–S3C). Early senescence was characterized by DNA damage response and p53 signaling, perhaps reflecting the first response to the damage caused by the radiation. Intermediate senescence was characterized by metabolic changes (the citric acid cycle and respiratory electron transport), p53-associated pathways, and signaling mediated by p38-gamma and p38-delta, two isoforms of p38-MAPK (mitogen-activated protein kinase) known to have an important role in senescence and the SASP [38]. Notably, only in late senescence were cell-cycle arrest and chromatin remodeling among the top differentially expressed pathways, surpassing other pathways in importance (Figure 3C). Interestingly, genes encoding SASP factors showed significant time-point- and cell-type-dependent heterogeneity (Figure 3D). This variability highlights the importance of time and cellular identity in determining the SASP and reflects the complexity of its regulation and biological functions [1].

Finally, we followed, over time, the 55 genes that constituted the senescence core signature (Figures 2B and 4). While we found differential expression of all the genes at day 10 for melanocytes and keratinocytes, other time points showed high variability. In the case of fibroblasts, the lack of significance of some genes at day 10 is likely due to the lack of power from using a single dataset, since these genes reached statistical significance only when multiple datasets were pooled. We also validated a subset of these genes in primary human HCA-2 fibroblasts and confirmed differential expression compared to that in proliferating and quiescent cells (Figures S4B and S4C). Nonetheless, among the 55 genes of the senescence core signature, 13 genes were differentially regulated at every time point and in every cell type (Figure 4, genes in red).

Many factors can influence the senescence program and the biological functions of senescent cells. Here, we investigated the senescence phenotypes related to 3 main variables: the stress signal, the type of cell, and the time after senescence induction. We found 1,311 genes uniquely differentially regulated in senescent fibroblasts and not quiescent fibroblasts. 55 genes were also shared among four different cell types induced to senesce by four different stimuli. The temporal dynamics of these genes exposed a new layer of complexity, revealing that the senescence signature found is highly time dependent. Nevertheless, we were able to identify 13 genes as differentially regulated in all the conditions considered, including time.

Among the known senescence-associated genes, we identified PATZ1, a transcriptional repressor that inhibits senescence [27], and CCND1, a regulatory subunit of CDK4 or CDK6 [29]. It is noteworthy that the common senescence markers, *CDKN2A*, *CDKN1A*, and *LMNB1*, were not within the core signature, supporting the idea that known senescence markers lack universality for different cell types and inducers of senescence [10]. Indeed, one of the studies used here [14] showed that p16INK4A mRNA levels are not always significantly changed in senescence in some fibroblast strains. Although RNA levels do not always reflect protein levels, p16INK4A expression is often used as a senescence marker. However, it is possible that samples collected to perform the RNA-seq experiments might have been in a pre-p16INK4A engagement phase, as p16INK4A is often induced late after senescence induction [39]. By contrast, p21CIP1 was among the genes differentially expressed by all senescent cell types and in response to all stimuli, although it was also slightly upregulated in quiescence, concordant with its known involvement in both types of cell-cycle arrest [40]. *LMNB1* was strongly downregulated in all cell types, with the exception of melanocytes, but was also somewhat downregulated at quiescence.

Finally, we showed that temporal dynamics strongly influence the detection of differentially expressed genes. In addition to the expression of the genes in our core signature, we included genes encoding known SASP factors (Figure 3D), further illustrating the heterogeneity among cell types and time points after

signature with genes differentially expressed ($p \leq 0.01$) in all three cell types and a shared IR-induced senescence (IRIS) signature with genes shared by all cell types and time points ($p \leq 0.01$) were generated.

(B) GO terms and pathways enriched in the shared IRIS signature among all time points and cell types. The figure shows enriched GO terms in the upregulated (red) and downregulated (blue) genes of the signature. Bars indicate the logarithm base 10 of the p value.

(C) Top 5 GO terms and pathways enriched at each time point. The figure shows the enriched GO terms and pathways for days 4, 10, and 20. Bars indicate the logarithm base 10 of the p value.

(D) Heatmap showing the dynamics of genes encoding SASP factors for each cell type. Known SASP factors that were significantly differentially expressed during at least one time point in each cell type are shown. The heatmap shows the logarithm base 2 of the fold change for each time post-irradiation with respect to proliferating cells. Quiescence was measured only on fibroblasts. The violet arrows highlight *MMP1*, the only SASP factor commonly regulated at days 10 and 20 in all cell types.

See Figure S4 and Data S3.

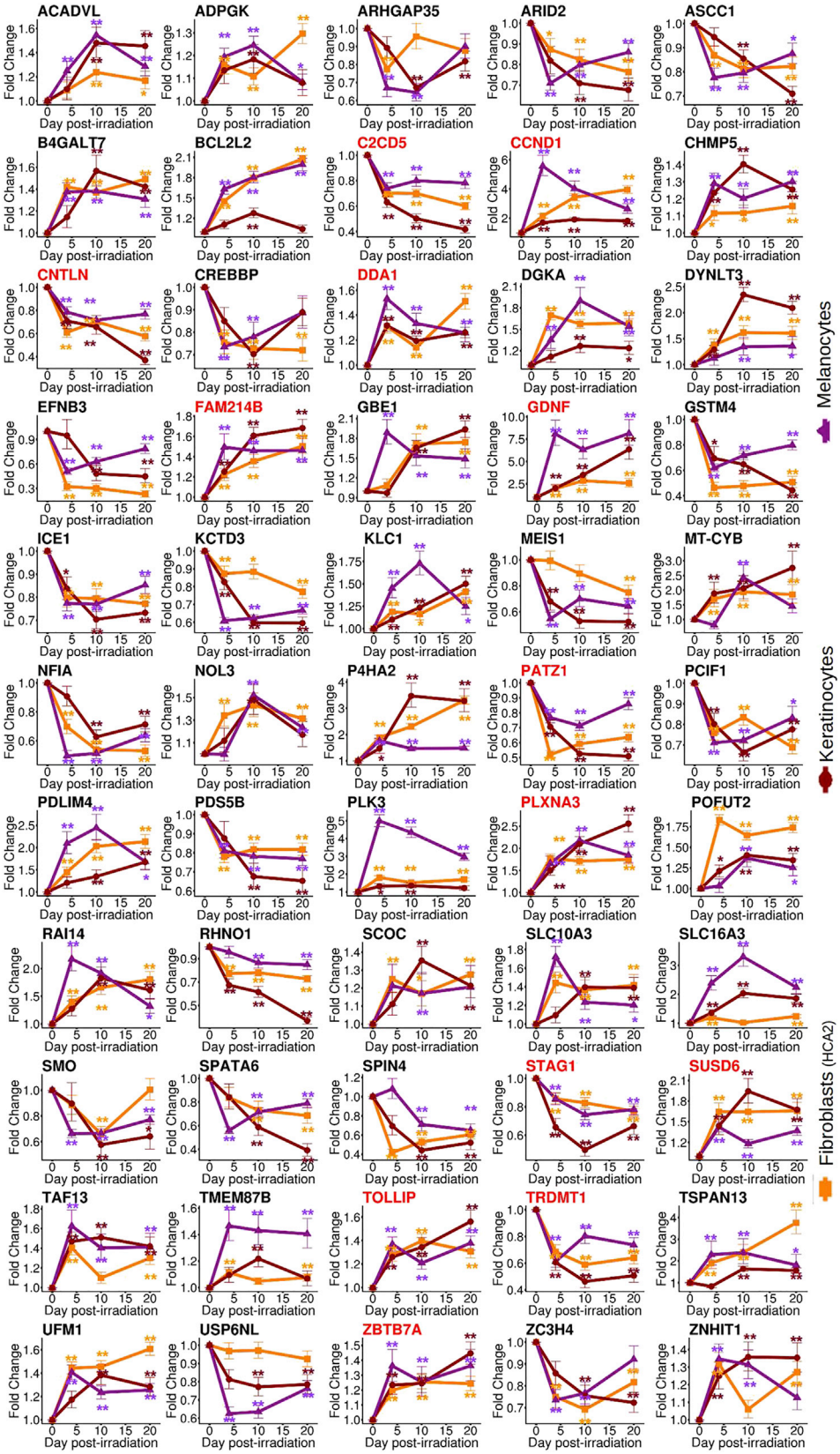

(legend on next page)

senescence induction. These findings emphasize the need to include time as a variable when studying senescence. It is clear, though, that there is, as yet, no universal marker of senescence. Others have proposed the use of multiple markers [10], and we propose here the use of core transcriptome signatures such as we provide here. These signatures can help identify senescent cells and discriminate among different senescence programs. The number of genes to be tested to achieve precision still needs to be determined, particularly in vivo. However, our data clearly highlight the heterogeneity of senescent cells in culture, anticipating that these challenges might be amplified in vivo, where less is known about the stimuli and cell types associated with senescence.

STAR★METHODS

Detailed methods are provided in the online version of this paper and include the following:

- KEY RESOURCES TABLE
- CONTACT FOR REAGENT AND RESOURCE SHARING
- EXPERIMENTAL MODEL AND SUBJECT DETAILS
  - Cell strains and culture
- METHOD DETAILS
  - Sample preparation
  - SA-βgal assay
  - EdU staining
  - Real Time-PCR
  - Public Datasets
  - RNaseq
  - Quality Control and Alignment of Sequencing Datasets
  - Meta-Analysis of Fibroblasts
  - Universal Senescence Signature shared in different Cell Types
- QUANTIFICATION AND STATISTICAL ANALYSIS
  - SA-βgal assay
  - EdU staining
  - Real Time-PCR
- DATA AND SOFTWARE AVAILABILITY
  - Self-generated RNaseq data
  - Plots

SUPPLEMENTAL INFORMATION

Supplemental Information includes four figures, one table, and three data files and can be found with this article online at http://dx.doi.org/10.1016/j.cub.2017.07.033.

AUTHOR CONTRIBUTIONS

Conceptualization, A.H.-S., J.C., and M.D.; Methodology, A.H.-S., V.G., and M.D.; Formal Analysis, A.H.-S., T.V.d.J., S.M., V.G., and M.D.; Investigation, A.H.-S., S.M., and M.D.; Writing – Original Draft, A.H.-S. and M.D.; Writing – Review & Editing, A.H.-S., V.G., J.C., and M.D.; Supervision, V.G., J.C., and M.D.; Funding Acquisition, J.C. and M.D.

ACKNOWLEDGMENTS

We would like to thank members of the Demaria lab for helpful discussion and support. A.H.-S. and M.D. are owners of a patent related to this work.

Received: January 2, 2017
Revised: June 22, 2017
Accepted: July 13, 2017
Published: August 24, 2017

REFERENCES

1. Loaiza, N., and Demaria, M. (2016). Cellular senescence and tumor promotion: is aging the key? Biochim. Biophys. Acta *1865*, 155–167.
2. Serrano, M., Lin, A.W., McCurrach, M.E., Beach, D., and Lowe, S.W. (1997). Oncogenic ras provokes premature cell senescence associated with accumulation of p53 and p16INK4a. Cell *88*, 593–602.
3. Muñoz-Espín, D., Cañamero, M., Maraver, A., Gómez-López, G., Contreras, J., Murillo-Cuesta, S., Rodríguez-Baeza, A., Varela-Nieto, I., Ruberte, J., Collado, M., and Serrano, M. (2013). Programmed cell senescence during mammalian embryonic development. Cell *155*, 1104–1118.
4. Storer, M., Mas, A., Robert-Moreno, A., Pecoraro, M., Ortells, M.C., Di Giacomo, V., Yosef, R., Pilpel, N., Krizhanovsky, V., Sharpe, J., and Keyes, W.M. (2013). Senescence is a developmental mechanism that contributes to embryonic growth and patterning. Cell *155*, 1119–1130.
5. Meyer, K., Hodwin, B., Ramanujam, D., Engelhardt, S., and Sarikas, A. (2016). Essential role for premature senescence of myofibroblasts in myocardial fibrosis. J. Am. Coll. Cardiol. *67*, 2018–2028.
6. Jun, J.I., and Lau, L.F. (2010). The matricellular protein CCN1 induces fibroblast senescence and restricts fibrosis in cutaneous wound healing. Nat. Cell Biol. *12*, 676–685.
7. Krizhanovsky, V., Yon, M., Dickins, R.A., Hearn, S., Simon, J., Miething, C., Yee, H., Zender, L., and Lowe, S.W. (2008). Senescence of activated stellate cells limits liver fibrosis. Cell *134*, 657–667.
8. Demaria, M., Ohtani, N., Youssef, S.A., Rodier, F., Toussaint, W., Mitchell, J.R., Laberge, R.M., Vijg, J., Van Steeg, H., Dollé, M.E., et al. (2014). An essential role for senescent cells in optimal wound healing through secretion of PDGF-AA. Dev. Cell *31*, 722–733.
9. Baker, D.J., Childs, B.G., Durik, M., Wijers, M.E., Sieben, C.J., Zhong, J., Saltness, R.A., Jeganathan, K.B., Verzosa, G.C., Pezeshki, A., et al. (2016). Naturally occurring p16(Ink4a)-positive cells shorten healthy lifespan. Nature *530*, 184–189.
10. Sharpless, N.E., and Sherr, C.J. (2015). Forging a signature of in vivo senescence. Nat. Rev. Cancer *15*, 397–408.
11. Liberati, A., Altman, D.G., Tetzlaff, J., Mulrow, C., Gøtzsche, P.C., Ioannidis, J.P.A., Clarke, M., Devereaux, P.J., Kleijnen, J., and Moher, D. (2009). The PRISMA statement for reporting systematic reviews and meta-analyses of studies that evaluate health care interventions: explanation and elaboration. J. Clin. Epidemiol. *62*, e1–e34.
12. Alspach, E., Flanagan, K.C., Luo, X., Ruhland, M.K., Huang, H., Pazolli, E., Donlin, M.J., Marsh, T., Piwnica-Worms, D., Monahan, J., et al. (2014). p38MAPK plays a crucial role in stromal-mediated tumorigenesis. Cancer Discov. *4*, 716–729.

Figure 4. Dynamic Changes in Expression of Genes in the Core Senescence Signature

Each panel shows one of the 55 genes in the core signature at the indicated points before and after irradiation. All genes show a dynamic temporal behavior at the time points tested: day 0 (proliferation), day 4, day 10, and day 20 after irradiation. Notably, all genes show a similar trend in the three cell types tested: fibroblasts (yellow), keratinocytes (red), and melanocytes (magenta). Genes in red correspond to those that reached significance ($p \leq 0.01$) at all time points tested. N = 6. $^{*}p \leq 0.05$; $^{**}p \leq 0.01$.

See also Figure S4 and Data S3.

13. Herranz, N., Gallage, S., Mellone, M., Wuestefeld, T., Klotz, S., Hanley, C.J., Raguz, S., Acosta, J.C., Innes, A.J., Banito, A., et al. (2015). mTOR regulates MAPKAPK2 translation to control the senescence-associated secretory phenotype. Nat. Cell Biol. *17*, 1205–1217.
14. Marthandan, S., Baumgart, M., Priebe, S., Groth, M., Schaer, J., Kaether, C., Guthke, R., Cellerino, A., Platzer, M., Diekmann, S., and Hemmerich, P. (2016). Conserved senescence associated genes and pathways in primary human fibroblasts detected by RNA-seq. PLoS ONE *11*, e0154531.
15. Marthandan, S., Priebe, S., Baumgart, M., Groth, M., Cellerino, A., Guthke, R., Hemmerich, P., and Diekmann, S. (2015). Similarities in gene expression profiles during in vitro aging of primary human embryonic lung and foreskin fibroblasts. Biomed Res. Int. *2015*, 731938.
16. Rai, T.S., Cole, J.J., Nelson, D.M., Dikovskaya, D., Faller, W.J., Vizioli, M.G., Hewitt, R.N., Anannya, O., McBryan, T., Manoharan, I., et al. (2014). HIRA orchestrates a dynamic chromatin landscape in senescence and is required for suppression of neoplasia. Genes Dev. *28*, 2712–2725.
17. Love, M.I., Huber, W., and Anders, S. (2014). Moderated estimation of fold change and dispersion for RNA-seq data with DESeq2. Genome Biol. *15*, 550.
18. Rau, A., Marot, G., and Jaffrézic, F. (2014). Differential meta-analysis of RNA-seq data from multiple studies. BMC Bioinformatics *15*, 91.
19. Kamburov, A., Wierling, C., Lehrach, H., and Herwig, R. (2009). ConsensusPathDB–a database for integrating human functional interaction networks. Nucleic Acids Res. *37*, D623–D628.
20. Kamburov, A., Pentchev, K., Galicka, H., Wierling, C., Lehrach, H., and Herwig, R. (2011). ConsensusPathDB: toward a more complete picture of cell biology. Nucleic Acids Res. *39*, D712–D717.
21. López-Otín, C., Blasco, M.A., Partridge, L., Serrano, M., and Kroemer, G. (2013). The hallmarks of aging. Cell *153*, 1194–1217.
22. Soto-Gamez, A., and Demaria, M. (2017). Therapeutic interventions for aging: the case of cellular senescence. Drug Discov. Today *22*, 786–795.
23. Fridlyanskaya, I., Alekseenko, L., and Nikolsky, N. (2015). Senescence as a general cellular response to stress: A mini-review. Exp. Gerontol. *72*, 124–128.
24. Coppé, J.-P., Patil, C.K., Rodier, F., Sun, Y., Muñoz, D.P., Goldstein, J., Nelson, P.S., Desprez, P.-Y., and Campisi, J. (2008). Senescence-associated secretory phenotypes reveal cell-nonautonomous functions of oncogenic RAS and the p53 tumor suppressor. PLoS Biol. *6*, 2853–2868.
25. Crowe, E.P., Tuzer, F., Gregory, B.D., Donahue, G., Gosai, S.J., Cohen, J., Leung, Y.Y., Yetkin, E., Nativio, R., Wang, L.-S., et al. (2016). Changes in the transcriptome of human astrocytes accompanying oxidative stress-induced senescence. Front. Aging Neurosci. *8*, 208.
26. Yosef, R., Pilpel, N., Tokarsky-Amiel, R., Biran, A., Ovadya, Y., Cohen, S., Vadai, E., Dassa, L., Shahar, E., Condiotti, R., et al. (2016). Directed elimination of senescent cells by inhibition of BCL-W and BCL-XL. Nat. Commun. *7*, 11190.
27. Cho, J.H., Kim, M.J., Kim, K.J., and Kim, J.R. (2012). POZ/BTB and AT-hook-containing zinc finger protein 1 (PATZ1) inhibits endothelial cell senescence through a p53 dependent pathway. Cell Death Differ. *19*, 703–712.
28. Breslin, L., Prosser, S.L., Cuffe, S., and Morrison, C.G. (2014). Ciliary abnormalities in senescent human fibroblasts impair proliferative capacity. Cell Cycle *13*, 2773–2779.
29. Burton, D.G., Sheerin, A.N., Ostler, E.L., Smith, K., Giles, P.J., Lowe, J., Rhys-Williams, W., Kipling, D.G., and Faragher, R.G. (2007). Cyclin D1 overexpression permits the reproducible detection of senescent human vascular smooth muscle cells. Ann. N Y Acad. Sci. *1119*, 20–31.
30. Demaria, M., O'Leary, M.N., Chang, J., Shao, L., Liu, S., Alimirah, F., Koenig, K., Le, C., Mitin, N., Deal, A.M., et al. (2017). Cellular senescence promotes adverse effects of chemotherapy and cancer relapse. Cancer Discov. *7*, 165–176.
31. Borràs-Fresneda, M., Barquinero, J.F., Gomolka, M., Hornhardt, S., Rössler, U., Armengol, G., and Barrios, L. (2016). Differences in DNA repair capacity, cell death and transcriptional response after irradiation between a radiosensitive and a radioresistant cell line. Sci. Rep. *6*, 27043.
32. Schafer, M.J., White, T.A., Iijima, K., Haak, A.J., Ligresti, G., Atkinson, E.J., Oberg, A.L., Birch, J., Salmonowicz, H., Zhu, Y., et al. (2017). Cellular senescence mediates fibrotic pulmonary disease. Nat. Commun. *8*, 14532.
33. Childs, B.G., Durik, M., Baker, D.J., and van Deursen, J.M. (2015). Cellular senescence in aging and age-related disease: from mechanisms to therapy. Nat. Med. *21*, 1424–1435.
34. Kim, Y.M., Byun, H.O., Jee, B.A., Cho, H., Seo, Y.H., Kim, Y.S., Park, M.H., Chung, H.Y., Woo, H.G., and Yoon, G. (2013). Implications of time-series gene expression profiles of replicative senescence. Aging Cell *12*, 622–634.
35. Schäuble, S., Klement, K., Marthandan, S., Münch, S., Heiland, I., Schuster, S., Hemmerich, P., and Diekmann, S. (2012). Quantitative model of cell cycle arrest and cellular senescence in primary human fibroblasts. PLoS ONE *7*, e42150.
36. Velarde, M.C., and Demaria, M. (2016). Targeting senescent cells: possible implications for delaying skin aging: a mini-review. Gerontology *62*, 513–518.
37. van Deursen, J.M. (2014). The role of senescent cells in ageing. Nature *509*, 439–446.
38. Xu, Y., Li, N., Xiang, R., and Sun, P. (2014). Emerging roles of the p38 MAPK and PI3K/AKT/mTOR pathways in oncogene-induced senescence. Trends Biochem. Sci. *39*, 268–276.
39. Stein, G.H., Drullinger, L.F., Soulard, A., and Dulić, V. (1999). Differential roles for cyclin-dependent kinase inhibitors p21 and p16 in the mechanisms of senescence and differentiation in human fibroblasts. Mol. Cell. Biol. *19*, 2109–2117.
40. Terzi, M.Y., Izmirli, M., and Gogebakan, B. (2016). The cell fate: senescence or quiescence. Mol. Biol. Rep. *43*, 1213–1220.
41. Demaria, M., Giorgi, C., Lebiedzinska, M., Esposito, G., D'Angeli, L., Bartoli, A., Gough, D.J., Turkson, J., Levy, D.E., Watson, C.J., et al. (2010). A STAT3-mediated metabolic switch is involved in tumour transformation and STAT3 addiction. Aging (Albany NY) *2*, 823–842.

STAR★METHODS

KEY RESOURCES TABLE

REAGENT or RESOURCE	SOURCE	IDENTIFIER
Chemicals, Peptides, and Recombinant Proteins		
DMEM, GlutaMAX Supplement, pyruvate	GIBCO	Cat#31966021
Dermal Cell Basal Medium	ATCC	Cat#ATCC PCS-200-030
Fetal Bovine Serum	GE Healthcare Bio-Sciences	Cat#SV30160.03
Pen/strep stock, 10,000/10,000, 100ml	Lonza	Cat#LO DE17-602E
Hydrogen Peroxide Solution	Sigma Aldrich	Cat#216763-100ML-D
Doxorubicin hydrochloride	Tebu-bio	Cat#BIA-D1202-1
25% Glutaraldehyde solution	Thermo Fisher Scientific	Cat#MERC8.20603.1000
16% Formaldehyde (w/v), Methanol-free	Thermo Fisher Scientific	Cat#28906
Diamidino-2-phenylindole (DAPI)	Sigma-Aldrich	Cat#D9542
Critical Commercial Assays		
Beta-Galactosidase Staining Kit	BioVision	Cat#K802
Click-iT EdU Alexa Fluor 488 Imaging kit	Thermo Fisher Scientific	Cat#C10337
Isolate II RNA Mini Kit	Bioline	Cat#BIO-52073
High-Capacity cDNA Reverse Transcription kit	Applied Biosystems	Cat#4368813
Universal Proble Library System	Roche	Cat#04683633001
SENSIFast Probe no-ROX One-step Kit	Bioline	Cat#BIO-76001
RNAeasy mini kit	QIAGEN	Cat#74104
Truseq RNA Sample Preparation kit	Illumina	Cat#RS-122-2001 or RS-122-2002
HiSeq PE Cluster Kit v4 – cBot	Illumina	Cat#PE-401-4001
HiSeq SBS Kit v4 (50 cycles)	Illumina	Cat#FC-401-4002
Deposited Data		
Self-generated RNA-seq datasets of IRIS in fibroblasts, melanocytes and keratinocytes	ArrayExpress database	ArrayExpress: E-MTAB-5403
Experimental Models: Cell Lines		
Human foreskin fibroblasts HCA2	O. Pereira-Smith (University of Texas Health Science Center, San Antonio)	N/A
Human foreskin fibroblasts BJ	ATCC	Cat#CRL-2522
Mouse Embryonic Fibroblasts (MEFs)	Self-produced	N/A
Mouse primary skin microvascular endothelial cells	Cellbiologics	Cat#C57-6064
Human Epidermal Keratinocytes Neonatal Foreskin	ATCC	Cat#PCS-200-010
Human Epidermal Melanocytes Neonatal	ATCC	Cat#PCS-200-012
Oligonucleotides		
Sets of primers for qPCR	IDT	Table S1
Software and Algorithms		
SRA Toolkit 2.6.2	GitHub	https://github.com/ncbi/sra-tools
FastQC software v0.11.5	Babraham Institute	https://www.bioinformatics.babraham.ac.uk/projects/fastqc/
Trimmommatic 0.36	Usadellab	http://www.usadellab.org/cms/?page=trimmomatic
STAR-2.5.1b	GitHub	https://github.com/alexdobin/STAR/releases
DESeq2	Bioconductor	https://bioconductor.org/packages/release/bioc/html/DESeq2.html
MetaRNaseq	CRAN	https://cran.r-project.org/web/packages/metaRNASeq/index.html
Consensus Path DB-human	Max Planck Institute	http://cpdb.molgen.mpg.de/

(*Continued on next page*)

Continued

REAGENT or RESOURCE	SOURCE	IDENTIFIER
R and associated R-packages (pheatmap, ggplot2, ggfortify, RcolorBrewer, VennDiagram)	Bioconductor, CRAN	https://cran.r-project.org/web/packages/
ImageJ	NIH – public domain	https://imagej.nih.gov/ij/download.html

CONTACT FOR REAGENT AND RESOURCE SHARING

Further information and requests for resources and reagents should be directed to and will be fulfilled by the Lead Contact, Marco Demaria (m.demaria@umcg.nl).

EXPERIMENTAL MODEL AND SUBJECT DETAILS

Cell strains and culture

Human foreskin fibroblasts HCA2 (male) were obtained from the laboratory of O. Pereira-Smith (University of Texas Health Science Center, San Antonio); human foreskin fibroblasts BJ were purchased from ATCC (Cat: CRL-2522); Human neonatal foreskin epidermal melanocytes and keratinocytes (male) were purchased from ATCC (Cat: PCS-200-012 and PCS-200-010, respectively). HCA2 cells were not re-authenticated by the laboratory, but regularly monitored for mycoplasma contaminations (once/2 weeks). Commercial cells were authenticated by ATCC. Mouse Embryonic Fibroblasts (MEFs – from unknown gender due to developmental stage) were produced from 13.5 day embryos as previously described [41]; mouse primary skin microvascular endothelial cells (gender not provided by the source) were purchased from Cellbiologics (Cat: C57-6064). All cells were cultured in 5% oxygen and 37C for at least 4 Population Doublings (PD) prior to use and tested regularly for mycoplasma infection. Fibroblasts were cultured in DMEM (Thermo Fisher Scientific) enriched with 10% fetal bovine serum (FBS, GE Healthcare Life Sciences) and 1% penicillin/streptomycin (Lonza). Endothelial cells were grown in an endothelial cell growth media (ATCC).

METHOD DETAILS

Technical and biological replications are described in the individual methods. Randomization and blinding of most experiments were not possible, but otherwise described. Statistical methods of computation are described in specific paragraphs. Inclusion and exclusion criteria for RNaseq datasets are provided in Data S1A.

Sample preparation

For each condition, 3 biological replicates were generated.

Quiescence was induced by culturing the cells for 48 hr in DMEM supplemented with 0.2% FBS.

For ionizing radiation-induced senescence (IRIS), cells were subjected to a 10 Gy dose of γ-radiation using a ^{137} Cesium source and medium was refreshed every 2 days. Cells were harvested at day 10 after irradiation for most of the experiments and validations. For the time series, cells were harvested at day 4, 10 and 20 after irradiation.

For replicative senescence (RS), cells were propagated in culture for ~4 months (re-cultured at 30%–40% density every time they reached 70%–80% confluency) until they stopped growing (~PD 65 for BJ cells).

For oxidative stress-induced senescence (OSIS), cells were treated with 200uM of hydrogen peroxide (Sigma Aldrich) for 2 hr, followed by drug removal and culturing in fresh DMEM supplemented with 10% FBS. Treatment was repeated at day 0, 3 and 6, with medium refreshed every 2 days in between, and cells harvested on day 10 after the first treatment.

Doxorubicin (Tebu-bio) was used in a concentration of 250 nM for 24 hr. The medium was then replaced by normal DMEM supplemented with 10% FBS and refreshed every 2 days. Cells were harvested on day 7 after treatment.

Proliferating controls for each condition were generated stimulating cells with the corresponding vehicles and/or considering the same PD of the treated samples. When only one control for multiple conditions is shown, it represents the average of controls for each condition.

SA-βgal assay

Cells were plated in a 24-well plate, fixed in a mixture of gluteraldehyde and formaldehyde (2%/2%) for 10-15 min and stained overnight with an X-Gal solution using a commercial kit (Biovision). Cells were counter-stained with a 1 μg/ml 4′,6-diamidino-2-phenylindole (DAPI, Sigma-Aldrich, D9542) solution for 20 min. Every biological replicate was stained in duplicate, and counting was made in blind.

EdU staining

Cells were cultured for 24 hr in the presence of EdU, and fixed and stain using a commercial kit (Click-iT EdU Alexa Fluor 488 Imaging kit; Thermo Fisher Scientific). Every biological replicate was stained in duplicate, and counting was made in blind.

Real Time-PCR

Total RNA was prepared using the Isolate II Rna Mini Kit (Bioline). 255 – 500 ng of RNA was reverse transcribed into cDNA using a kit (Applied Biosystems). qRT-PCR reactions were performed as described [1] using the Universal Probe Library system (Roche) and a SENSIFast Probe kit (Bioline). Expression of tubulin was used to normalize the expression of CT values. List of primers used is provided as Table S1. Every biological replicate was analyzed in duplicate.

Public Datasets

A summary of the selection of the datasets and the samples used can be found in Data S1A. The raw data for the different public datasets used was collected from the "GEO repository" (https://www.ncbi.nlm.nih.gov/geo/). Five public datasets studying the transcriptome of senescent fibroblasts were included: 1) Alspach et al. (ID code: GSE56293) used RS in BJ cells as a model to study SASP induction. 2) Herranz et al. (ID code: GSE61130) studied the control of SASP factors in an OIS (induced by Ras) model in IMR90 cells. 3) Marthandan et al. [2] (ID code: GSE64553) used five different strains of fibroblasts (BJ, WI-38, IMR90, HFF and MRC-5 cells) to study RS. 4) Marthandan et al. [1] (ID code: GSE63577) used MRC-5 and HFF cells to study the effect of rotenone in different PD. Only the first (proliferation) and last time point (RS) for HFF cells were used. 5) Rai et al. (ID code: GSE53356), used IMR90 cells to study the chromatin landscape of RS. One public dataset produced by Crowe et al. (ID code: GSE58910) studying OSIS in astrocytes was used for the core signature of senescence shared by different cell types. The ID code for this dataset is: GSE58910.

RNaseq

Cells (6 biological replicates per condition) were prepared for RNA extraction via an RNAeasy mini kit (QIAGEN). Samples were treated with Qiasol lysis buffer and extracted for total RNA on a Qiacube robot per the manufacturer's instructions (Invitrogen). The extracted RNA was quantitated using a NanoDrop (higher than 1 μg) and RNA quality was measured via BioAnalyzer chip (Agilent) (RIN of 8 or greater). Purified RNA samples were then sent to the University of Minnesota BioMedical Genomics Center for Illumina HiSeq RNA sequencing, where RNA-Seq library preparation was carried out using Illumina's Truseq RNA Sample Preparation kit (Cat. # RS-122-2001 or RS-122-2002) according to the manufacturer's protocols. Briefly, RNA was oligo-dT purified using oligo-dT coated beads and then reverse transcribed into cDNA. The cDNA is fragmented, blunt-ended, and indexed (barcoded) adaptors are ligated to the ends of the fragments that are then amplified using 15 cycles of PCR. The final library size distribution was validated using capillary electrophoresis and quantified using fluorimetry (PicoGreen) and via qPCR. Indexed libraries are then normalized, pooled and size selected to 320bp ± 5% using Caliper's XT instrument. Samples were then paired-sequenced on the Illumina HiSeq 2000 System using Illumina's HiSeq PE Cluster Kit v4 – cBot (PE-401-4001) HiSeq SBS Kit v4 (50 cycles) (FC-401-4002). For the primary analysis and de-multiplexing, base call (.bcl) files for each cycle of sequencing are generated by Illumina Real Time Analysis (RTA) software. Primary analysis and de-multiplexing were performed using Illumina's CASAVA software 1.8.2. Average Quality scores for the completed run across all samples was > 30, with an average number of reads for each pooled sample greater than 10 million reads.

Quality Control and Alignment of Sequencing Datasets

Raw data of the public datasets was downloaded as fastq files using the SRA Toolkit 2.6.2. Quality control of all samples, including our own, was performed using the FastQC software v0.11.5 and the low quality reads (Average Quality: < 20) were discarded. End-trimming was performed when necessary by using the tool Trimmommatic 0.36. Samples were aligned to the GRCh38 genome using STAR-2.5.1b aligner and a count table was directly obtained with Star. Only genes annotated as protein-coding were included in the analysis.

Meta-Analysis of Fibroblasts

The heterogeneity of the data was evaluated with a Principal Component Analysis (PCA)-plot of the log-transformed normalized counts for the protein-coding genes, evaluating whether they clustered with similar samples in the same dataset.

For the meta-analysis (both for RS and for the senescence signature for fibroblasts), we used three different methods: negative-binomial generalized linear model (GLM), Fisher p value combination and Inverse Normal p value combination. In the case of the senescence signature for fibroblasts, we included all the samples in one unique meta-analysis. The first approach for the meta-analysis used the R-package DESeq2 for differential expression analysis. We included two variables in the model: a) Condition: senescence versus proliferation as the main variable of the model; b) Batch: we created this covariate to account for the differences in cell strain and the study they belonged to. In this variable, an identifier was assigned to each set of samples that belonged to the same dataset and same cell strain. Thus, every dataset included as many identifiers as number of cell strains used. The other two approaches were done by analyzing each dataset individually using DESeq2 to later combine the p values of the results by using the R-package MetaRNaseq. Therefore, the second approached used a Fisher- and the third one an Inverse Normal-p value combination. Genes with an adjusted p value $\leq$ 0.01 in the negative-binomial GLM and a combined p value $\leq$ 0.01 in the other two methods were included in the corresponding signature.

Genes that were also differentially regulated in the quiescence samples (adjusted p value $\leq$ 0.01 and sign of the fold change in the same direction than senescence) were removed from the list of possible senescence markers after each meta-analysis was finished.

Enriched pathways and Gene Ontology (G.O.) terms in the differentially expressed genes within the "Fibroblast Senescence signature" were evaluated by using the online tool "Over-representation analysis" of the Consensus Path DB-human (http://cpdb.molgen.mpg.de/) [19, 20].

Universal Senescence Signature shared in different Cell Types

Differential Expression analysis was also performed with DESeq2 for each individual dataset separately and the gene lists of differentially expressed genes were compared to the senescence signature of fibroblasts, without combining their p values. As before, only genes with a p value ≤ 0.01 in every dataset and within the signature of fibroblasts were included in the core senescence signature.

QUANTIFICATION AND STATISTICAL ANALYSIS

SA-βgal assay

Images were acquired at 100X magnification, and the number of cells counted by the software ImageJ (http://www.rsbweb.nih.gov/ij/). The number of positive cells was counted manually in blind.

EdU staining

Images were acquired at 400X magnification, quantified using ImageJ (http://www.rsbweb.nih.gov/ij/). In all cases, both for SA-βgal assay and for EdU staining, samples were done in triplicates and at least 100 cells were counted in each replicate (in blind) and corresponding barplots were generated, where error bars represent the Standard Error of the Mean (SEM).

Real Time-PCR

Tubulin was used for normalization of the CT values. All samples were run with a technical replicate and in 2-3 biological replicates. An unpaired two-tailed Student's t test was used to determine statistical significance based on delta-CT values. P values of 0.05 or less were considered statistically significant.

DATA AND SOFTWARE AVAILABILITY

Self-generated RNaseq data

RNaseq data has been deposited in the ArrayExpress database (http://www.ebi.ac.uk/arrayexpress) under ID code ArrayExpress: E-MTAB-5403.

Plots

All plots were made in R using the following R-packages: "pheatmap," "ggplot2," "ggfortify," "RColorBrewer" and "VennDiagram."